Stereo Camera Simulation for Lunar Surface Photogrammetry

Ryan J. Thompson[*], Paul M. Danehy[†], Michelle M. Munk[‡]
NASA Langley Research Center, Hampton, VA 23681

Manish Mehta[§] and Michael S. Manginelli[**]
NASA Marshall Space Flight Center, Huntsville, AL 35812

Chi Nguyen[††]
Aerospace Innovations, LLC, Yorktown, VA 23692

Orrin H. Thomas[‡‡]
Cardinal Systems, LLC, Flagler Beach, FL 32136

During the rocket-powered landing of a vehicle on a planetary body, the interaction between the rocket plume and the surface material beneath the vehicle plays a significant role in the descent dynamics and the safety of powered descent. However, *in situ* data taken to investigate plume-surface interaction has been limited. The upcoming flight and lunar landing of the Intuitive Machines *Nova-C* will be equipped with the Stereo Cameras for Lunar Plume-Surface Studies (SCALPSS) science package, enabling the direct measurement of plume-induced surface cratering during powered descent. In this work, we present the engineering constraints, design iteration process, and simulation results that drove the design selection for the SCALPSS camera system. The chosen design will provide 3D-imaging coverage of 84 percent of the lunar surface directly under the landed *Nova-C*, in addition to some coverage of the neighboring surface. SCALPSS will provide a total 3D-imaging coverage area of approximately 13 square meters. With the anticipated *Nova-C* landing in October of 2021, SCALPSS will provide the first dedicated in-situ measurement of plume-induced surface cratering.

I. Nomenclature

h	=	mounting height of cameras, measured from ground when the lander is resting on the lunar surface
R	=	mounting radius of cameras
α	=	twist angle of cameras about optical axis
β	=	rotation angle of whole camera system about the lander body axis
θ	=	angular coordinate of cameras, measured from the y-axis

---

[*] Aeronautics Research Intern, Advanced Measurements and Data Systems Branch and PhD Student, Department of Mechanical and Aerospace Engineering, University of Virginia, Charlottesville, VA.
[†] Senior Technologist for Advanced Measurement Systems, Advanced Measurements and Data Systems Branch, AIAA Associate Fellow.
[‡] SCALPSS Principal Investigator, Space Technology and Exploration Directorate, AIAA Associate Fellow.
[§] Aerothermodynamics Subject Matter Expert, Aerosciences Branch, AIAA Senior Member.
[**] Aerospace Engineer, Aerosciences Branch, AIAA Member.
[††] Principal Scientist.
[‡‡] Software Engineer.

ϕ	=	rotation of camera orientation about local x-axis
ω	=	rotation of camera orientation about local y-axis

II. Introduction

The interaction between a spacecraft descent engine exhaust plume and loose surface material during powered landing is not well-understood but plays a significant role in landing dynamics. Plume-surface interaction (PSI), and the ejection of surface material, or regolith, can pose a danger to the landing system and the environment in the vicinity of the landing site. Plume-induced ejecta can obscure the spacecraft's view of the landing site, adding to the difficulty and danger of crewed and uncrewed landings [1, 2, 3]. The ejecta can also be detrimental to the performance of landing sensors, such as radar and lidar, which are critical to the safety of autonomous landings [3]. Historically, fast-moving ejecta has inflicted damage upon several landing systems, including the Apollo landers and the Mars Science Laboratory [2]. Additionally, the rocket plume and resulting ejecta have the potential to erode and otherwise disturb the landing site and surrounding area. This is especially relevant when planning for the landing of several spacecraft within a small region (or lunar "base"), as is being considered for the Artemis program [4]. During previous lunar and Martian landings, cratering in regolith directly under the descent engine(s), caused by plume-surface interactions, has been observed to occur (Fig. 1). While several previous studies have investigated PSI during landings on the Moon and Mars using existing data, to date there have been no dedicated instruments for studying PSI flown on landing craft [3, 5]. Terrestrial PSI experiments can give some insight to the physics involved, but often these studies do not reflect the atmospheric and flow conditions present in extraterrestrial landings [1]. The lack of dedicated in-flight PSI data has hindered the development of accurate PSI simulation tools. This motivates the design and implementation of flight hardware for the *in situ* investigation of extraterrestrial PSI.

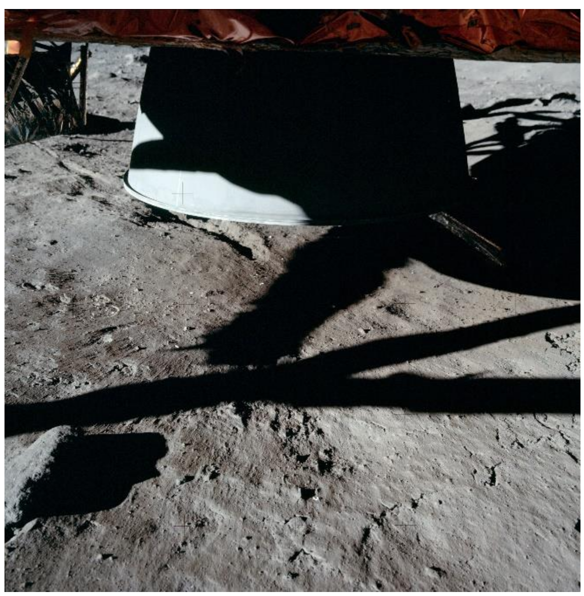

Fig. 1 Region of lunar surface under the Apollo 11 descent engine (top middle). The top layer of loose regolith has been swept away by the plume of the engine, exposing the underlying rock and creating a small crater. Courtesy of NASA.

The Stereo Cameras for Lunar Plume-Surface Studies (SCALPSS) science package is a set of PSI diagnostic hardware to be included in the payload of the Intuitive Machines *Nova-C* robotic lander on its mission to the lunar surface. SCALPSS is a set of four cameras that will view the region under the lander during and after landing, allowing for the 3D reconstruction of the post-landing lunar surface via photogrammetry. In this work, the process of designing and simulating the performance of the SCALPSS camera system is described. The simulations presented here employ use of the Virtual Diagnostic Interface (ViDI) technique, first described by Schwartz [6]. ViDI allows virtual cameras to be placed on a 3D model of the *Nova-C* lander, providing accurate estimates of camera fields-of-view and thus photogrammetry coverage. The design periods of the *Nova-C* and the SCALPSS camera system were concurrent, and design changes of the lander often affected the design of SCALPSS. The use of ViDI allowed these design changes to be incorporated quickly, enabling near-immediate analysis of changes in the simulated performance of SCALPSS that resulted from the lander design changes. These simulations of the SCALPSS camera system proved to be a crucial asset throughout its design process.

III. SCALPSS Mission

A. Overview

NASA's Commercial Lunar Payload Services (CLPS) program provides an opportunity for dedicated PSI instrumentation to be delivered to the Moon on a commercial lunar lander. In response to this opportunity, the SCALPSS imaging system is being designed and prepared for flight on the Intuitive Machines *Nova-C*, scheduled for launch in October of 2021. SCALPSS is being developed by NASA Langley Research Center, in collaboration with NASA Marshall Space Flight Center with assistance from the Jet Propulsion Laboratory. The SCALPSS imaging system consists of four cameras mounted along the base of the *Nova-C* lander body, pointed directly under the descent engine. This camera arrangement will provide multiple stereoscopic views of the area under the lander, enabling quantitative photogrammetric measurement of the plume-induced crater in the regolith that will form during landing. Photogrammetry is a technique that allows the 3D shape of an object to be measured by imaging the object from multiple perspectives with a camera, effectively providing a stereo view of the object [5, 7]. The SCALPSS system will be used to measure the volume of regolith displaced by the descent engine plume during and after landing. This measurement will provide valuable information about the rate of regolith ejection and the geometry of the plume-induced crater, which will aid in the development and validation of PSI models.

The SCALPSS cameras will begin acquiring images during the descent of the lander, 30 seconds before touchdown. Image acquisition will continue throughout descent and after landing. The four cameras will be synchronized with a common trigger source, so that all four images (one from each camera) will be acquired simultaneously. The post-landing acquisition phase will last several hours, allowing regolith ejected during landing to settle and the solar illumination angle to change. After landing, the full-resolution images from each camera acquired throughout the landing process will be transmitted to Earth for processing. A cartoon of the pre- and post-landing configurations is shown in Fig. 2. Each set of four simultaneous images will be used to photogrammetrically reconstruct the 3D shape of the lunar surface under the *Nova-C* before and after landing. This, in turn, will provide a measure of the amount of regolith displaced by the descent engine exhaust.

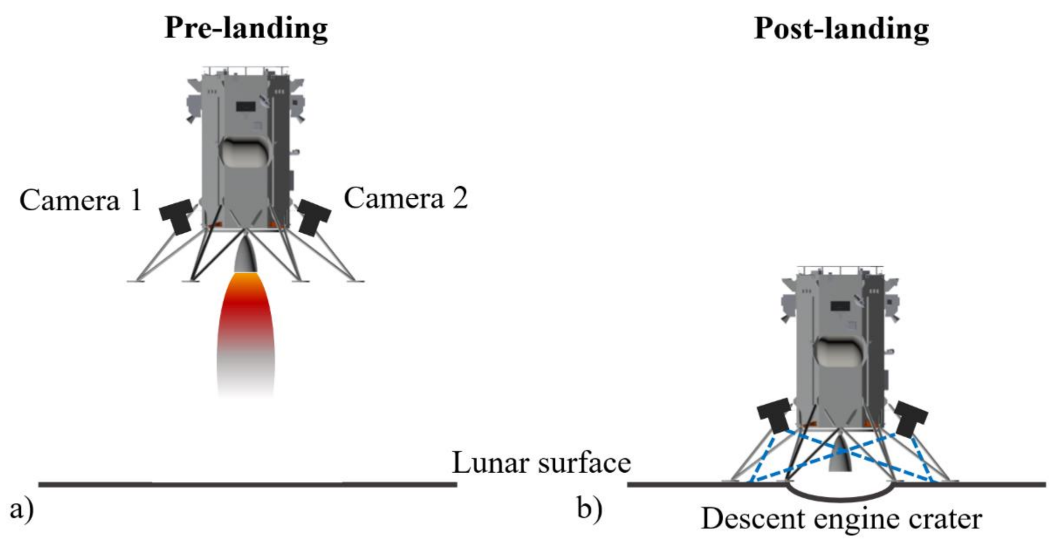

Fig. 2 a) The *Nova-C* during the descent phase, with the engine exhaust plume and SCALPSS cameras (size exaggerated for clarity) shown. b) The *Nova-C* post-landing, with the plume-induced crater (depth exaggerated for clarity) and SCALPSS camera fields-of-view (blue dashed lines) shown.

SCALPSS is comprised of several hardware elements mounted at various locations on the *Nova-C* lander. The cameras are FLIR Chameleon3 with 3.2 MP CMOS sensors (CM3-U3-31S4M-CS) and 3.37 mm focal length lenses (Peau Productions GP33728). Camera brackets mount the cameras to the lander body and position them at a specified location and orientation. Power and data connections for the cameras meet at a USB hub, which in turn transmits the image data to a data storage unit (DSU). Models of these components, mounted on the *Nova*-C lander, are shown in Fig. 3. After landing, the *Nova-C* will transmit the image data stored on the DSU to Earth.

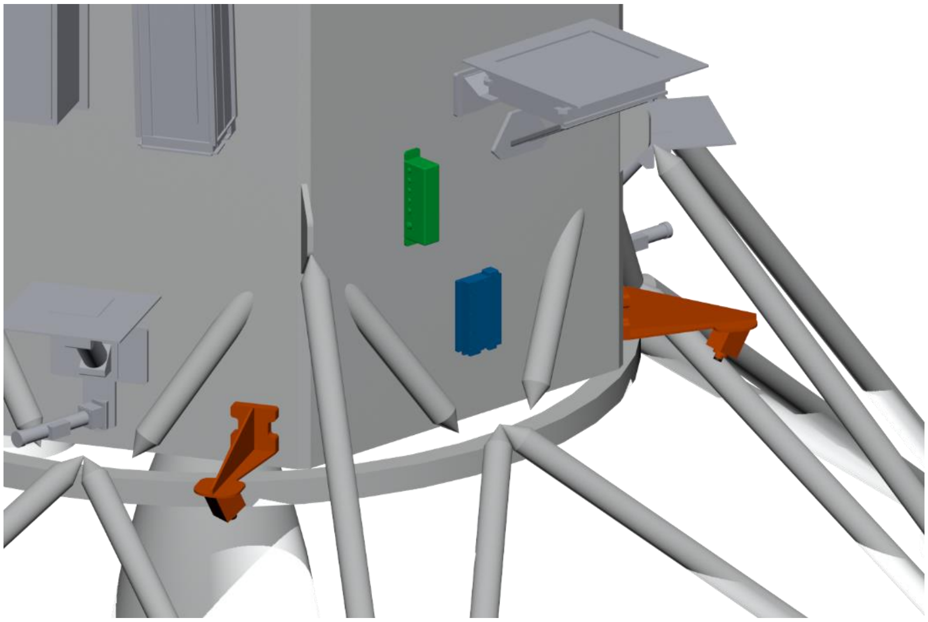

Fig. 3 The placement of the SCALPSS cameras and camera brackets (orange), USB hub (green), and data storage unit (blue). Only two of the cameras are visible in this view; the other two cameras are located on the opposite side of the lander. The cables connecting the cameras, USB hub, and data storage unit are not shown.

B. Requirements

The success of the SCALPSS system depends on each of the four cameras having an unobstructed view of the lunar surface below the lander, which necessitates careful integration of the cameras with the *Nova-C* lander. The landing system employed by the *Nova-C* consists of a single descent engine and 6 equally spaced landing legs. The structure of the lander allowed a large degree of flexibility in the placement of the SCALPSS cameras. This flexibility permitted the optimization of the camera system design, but the large available design space necessitated a simulation scheme for accurately and quickly evaluating the performance of many candidate configurations. Additionally, the camera system was subject to several engineering constraints, which further complicated the design process.

Several design constraints were present at the beginning of the design process, and several others were added later in the process as new information about the *Nova-C* and SCALPSS hardware became available. Here, these constraints are listed in the approximate order of priority. The most critical constraint required that the SCALPSS system not harm the host *Nova-C* lander. The success of SCALPSS, from a scientific perspective, required that SCALPSS provide 3D imaging (photogrammetry) covering at least 50% of the plume-induced crater with an accuracy of 0.25 cm. Additionally, SCALPSS must identify plume-surface erosion features to inform the development of PSI models. To ensure the accuracy of photogrammetry results, there must be sufficient distance between two cameras in a stereo pair. If a pair of cameras are very close together, they will provide less accurate results than a pair of cameras spaced further apart. The potential for damage to the cameras due to the engine exhaust and ejected regolith was mitigated by requiring that the cameras be mounted near to the lander body and as far above the ground is possible—outside of the main region of plume-surface interaction. The cameras were also required to not be directly below the *Nova-C* stage adapter, visible just below the camera brackets in Fig. 3. This region is where the *Nova-C* mounts to its launch vehicle, and thus must be kept free of obstructions. Two of the four cameras with overlapping fields of view were required to be shaded from the Sun by the lander body during and immediately after landing, in order to prevent those cameras from being damaged by solar heating after landing. This ensures that if the two cameras exposed to sunlight are damaged, the other two cameras will remain functional. It was also desired to mount the cameras near to the 'spines' of the lander body—that is, near the vertical edges of the lander where the landing legs also mount. These spines are especially rigid regions of the lander body, and thus provide desirable mounting locations for the SCALPSS cameras. The four camera mounts were required to be either identical in geometry or mirror images of each other. This requirement served to reduce the amount of time needed to design and manufacture the camera mounts. The final requirement of the camera system was that the six *Nova-C* landing feet should be visible to the cameras, which would allow the cameras to monitor any deformation of the landing legs that occurs during touchdown on the lunar surface. These constraints, in addition to the desire for maximal photogrammetric coverage of the ground under the lander, drove the entire design process. This challenging design environment motivated the use of computer-generated camera view simulations that incorporated the 3D model of the lander, which is the focus of the work presented here.

C. Design Timeline

Due to the timeline of the SCALPSS project, the design phase for the SCALPSS camera system was concurrent with the design of the *Nova-C* lander. This required SCALPSS to adopt an adaptive design process that could incorporate regular lander design changes at a fast pace. In the early stages of the camera system design (mid-2019), no official 3D geometry model of the *Nova-C* was available for analysis. Thus, an approximate 3D model for the lander was created based on the dimensions that were available. This model, deemed version 0.1 in Table 1, served as a surrogate for the actual lander geometry while we developed simulation techniques in ViDI that would allow us to evaluate camera system designs. Proof-of-concept photogrammetry coverage simulations were conducted with this version. In late 2019, version 0.5 of the *Nova-C* geometry was provided to us by Intuitive Machines. In the ViDI environment, the version 0.1 model was replaced with the new version 0.5 model, and we began testing camera configurations with the updated geometry. While this analysis helped inform some design decisions, the version 0.5 geometry was still fairly primitive and approximate. The version 1.0 geometry was released by Intuitive Machines in January of 2020 and was the first high-fidelity model available to us. The level of detail present in version 1.0 was a significant improvement over the previous version 0.5 geometry. The version 1.0 geometry was the primary model used during the SCALPSS design process, and with this geometry, the locations and orientations of each camera were selected. Versions 0.1, 0.5, and 1.0 are shown in Fig. 4. Later model versions (1.1 and 1.2) introduced only slight changes to the version 1.0 geometry, and thus prompted slight changes to the design of the camera configuration. For each of the model version changes, the new geometry could be quickly imported into the ViDI simulation environment and integrated with the existing camera system design to evaluate the performance of the design with the new lander model. Depending on the simulated performance of the camera system, the camera system design can be modified to better integrate with the lander geometry. As an example, version 1.1 featured a lander body that was slightly closer to the ground than in version 1.0. Consequently, the version 1.1 lander body obscured a significant portion of the cameras' fields of view. This was corrected by slightly lowering the mounting height of all four cameras (discussed further in Section V. B.). In conjunction with the lander geometry changes, the camera system design constraints also changed throughout the project. The ViDI environment facilitated prompt implementation of these changes and analysis of the resulting design implications.

Table 1 Version history of the *Nova-C* 3D geometry used for SCALPSS simulations and design.

Model Version	Date Released by IM	Notes
0.1	N/A (used July-October 2019)	Simplistic model based on images of *Nova-C* lander from Intuitive Machines' website; for model development and preparation for actual lander geometry model
0.5	October 2019	First geometry model provided by Intuitive Machines; included approximate dimensions for preliminary planning
1.0	January 31, 2020	First high-fidelity model provided by Intuitive Machines; included greater detail than version 0.5 and introduced a hexagonal lander body core
1.1	April 3, 2020	Decreased distance of engine bell and bottom of lander body from ground when landed
1.2	July 10, 2020	Slight increase in lander body diameter and decrease in distance between bottom of lander body and ground

D. Pre-Flight Testing of SCALPSS system

In addition to the camera system simulations presented here, additional tests confirming the performance of the SCALPSS design have been conducted. In the early stages of the design process, Marshall Space Flight Center (MSFC) employed its own simulation environment, created by Cardinal Systems, that allowed various camera configurations to be tested. The results of these simulations, an example of which is shown in Fig. 5 (a), were plots of camera fields of view projected onto the ground. These plots provided useful information about the size of the region that is accessible to photogrammetry. However, the geometry of the lander was not considered in these simulations, so field-of-view obstructions due to the descent engine, landing legs, and lander body were not accounted for. The ViDI environment described here did account for these obstructions, and a resulting photogrammetry coverage plot for the same camera arrangement as NASA MSFC simulated can be found in Fig. 5 (b). Thus, our simulations and the independent simulations conducted by MSFC allowed us to evaluate the validity of results from both sources. The two coverage maps shown provide similar information, but Fig. 5 (b) has accounted for obstructions to the SCALPSS cameras' fields of view due to the *Nova-C* geometry. As an example, the "U" shaped regions in 5(b) are regions shadowed by the nozzle bell, not captured in the MSFC simulation. When this obstruction is not accounted for, as in Fig. 5 (a), the simulation over-estimates the total coverage area by approximately 50% when compared to the simulation that does account for obstructions (Fig. 5 [b]). This example underscores the importance of including the *Nova-C* geometry in the SCALPSS coverage simulations.

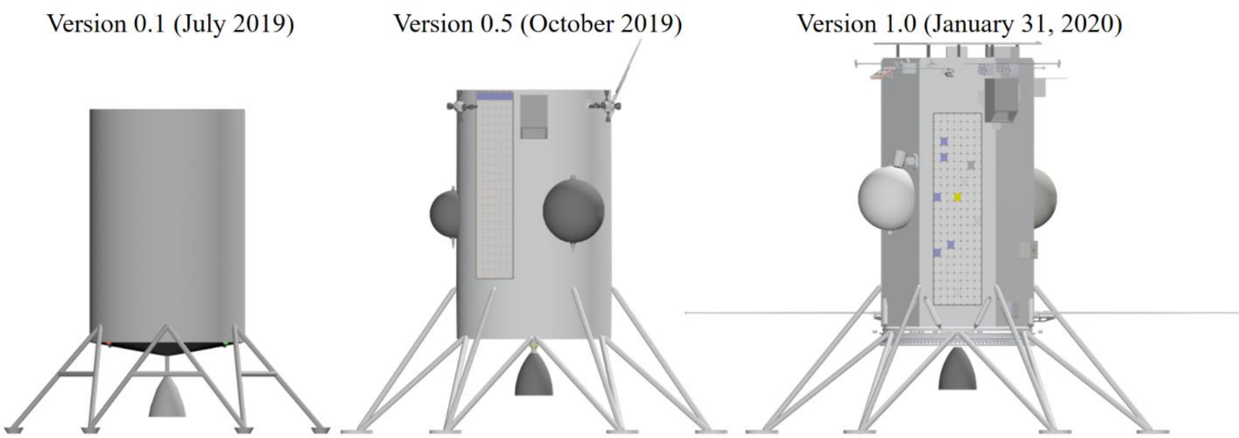

Fig. 4 The first three iterations of the *Nova-C* lander geometry used in ViDI simulations of the SCALPSS camera system.

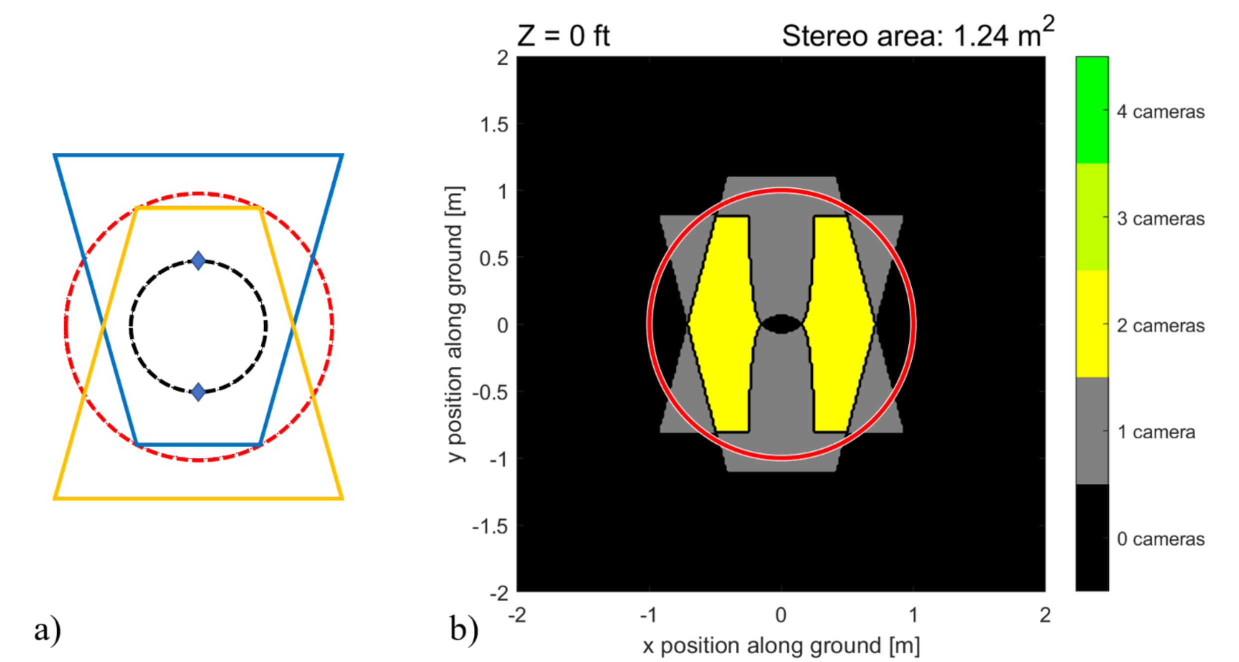

Fig. 5 a) An example two-camera photogrammetric coverage map created with the simulation environment developed by MSFC. The blue diamonds are the camera mounting locations, the black dashed circle is camera mounting radius, the red dashed circle is the photogrammetric area of interest, and the blue and yellow trapezoids are the projected fields of view of the two cameras. The overlapping region between the camera

fields of view is accessible to photogrammetry. b) A photogrammetric coverage map for a camera configuration similar to (a), created with the simulation environment described here. The red circle is the area of interest and the color scale quantifies the number of cameras that can 'see' a given point on the ground. Note that the mounting locations of the cameras differed slightly between the two simulations shown here.

IV. Simulation Environment

A. Camera Placement Nomenclature

Positioning and orienting the cameras in 3D space around the lander model required a common coordinate system to be defined. We chose symmetric polar coordinates to define the locations of each camera, in order to meet the design constraint that the mounts for both pairs of cameras must be either identical or exhibit mirror symmetry. The *x*- and *y*-axes were chosen such that they will point in the east and north directions, respectively, post-landing on the Moon. All four cameras were located the same distance R from the center axis of the lander body. The vectors describing the positions of each camera formed an angle θ with the +*y*- or -y-axis, as shown in Fig. 6 (a). The mounting height of all four cameras was h, which was the distance along the *z*-axis between the cameras and the ground plane (post-landing). We also allowed the group of cameras as a whole to rotate about the *z*-axis by an angle β. As an example, a rotation of $\beta = 90°$ would move the camera in the (+*x*, +*y*) quadrant into the (-*x*, +*y*) quadrant, the camera in the (-*x*, +*y*) quadrant into the (-*x*, -*y*) quadrant, and so on. R, θ, h, and β fully define the positions of the cameras. To specify the orientations of the cameras, we introduce the variables α, ϕ, and ω. The angle α describes rotations of the cameras about their optical axes, while ϕ and ω are the angles of rotation of the camera about the local *x*- and *y*-axes, respectively (see Fig. 6 [b]). The variables ϕ and ω for each camera were designated to be positive when they cause the cameras to point toward the vertical centerline of the lander. When $\phi = \omega = 0$, the cameras are pointing vertically down, along the +*z*-axis. As shown in Fig. 6 (b), both ϕ and ω are positive. Thus, with the notation presented here, the positions and orientations of all four cameras are fully defined.

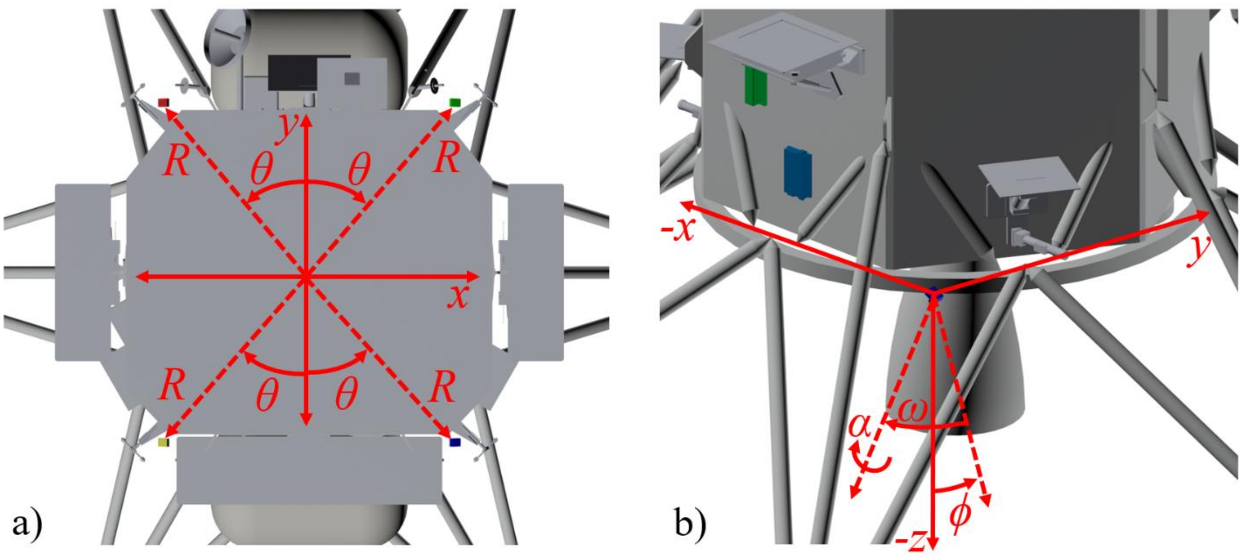

Fig. 6 a) Top view of the coordinate system used to define the locations of the cameras. The colored rectangles at the end of each dashed vector are the camera bodies, drawn to scale. b) Isometric view of the coordinate system used to define the orientations of the cameras. As shown, the camera is first rotated by ϕ about the *x*-axis, then by ω about the *y*-axis, and finally by α about its optical axis.

B. 3D Configuration Simulation

Central to the ViDI simulation environment is Autodesk 3ds Max, a 3D computer modeling application. This software enables users to create realistic scenes that incorporate lights, shadows, 3D models, cameras, textures, animation, and other features useful for experiment-planning purposes. Autodesk 3ds Max supports a native macro programming language, entitled MAXScript, which can aid in automating processes such as positioning objects and performing renderings from the SCALPSS cameras as well as artificially placed non-SCALPSS cameras. A Cartesian coordinate system can be used for precise placement of objects in the scene. By recreating the *Nova-C* lander and

SCALPSS assembly in this environment, we were able to simulate the views of camera and the region of ground under the lander that would be accessible to photogrammetry.

To create this scene in Autodesk 3ds Max, the *Nova-C* CAD geometry file was imported, and the rest of the scene was built around it. A plane approximating the lunar surface was placed directly under the lander model, coincident with the bottom of the lander footpads. This plane served as the viewing target of the virtual cameras. Fig. 7 (a) provides an example view of this scene. Four virtual cameras were created with characteristics identical to the actual flight cameras: a 7.1 mm by 5.3 mm image sensor with 2048 by 1536 pixels, and a lens focal length of 3.37 mm. The locations and orientations of each of the cameras was set by a MAXScript macro that took as inputs the position descriptors R, θ, h, and β and the orientation descriptors α, ϕ, and ω, and calculated the Cartesian coordinates and Euler angles that described the pointing direction of the cameras. Using the calculated coordinates and Euler angles of each camera, the macro placed the cameras at their corresponding positions in the scene. This system of automatically placing the cameras was beneficial for two reasons: it allowed repeatable, high-accuracy placement of each camera, and it could easily be adapted to performing simulations in a batch mode. When testing many different camera system designs, this batch processing technique proved essential, allowing thousands of camera configurations to be simulated to optimize the design.

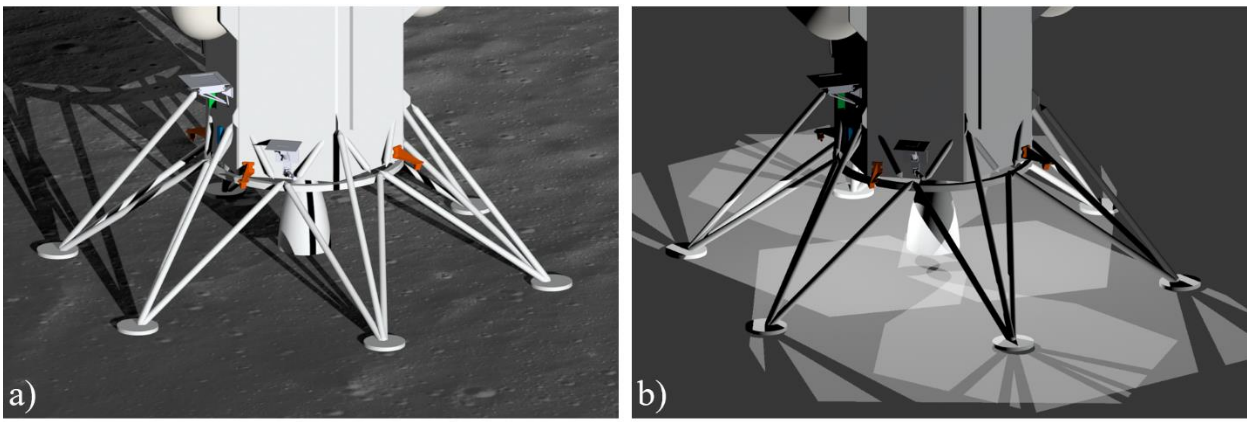

Fig. 7 a) View of Autodesk 3ds Max scene with simulated sunlight and shadows, and a textured ground plane. The SCALPSS camera brackets are shown in orange. b) The same scene and perspective as shown in (a), but with no sunlight, a flat gray ground plane, and the projected fields of view from the SCALPSS cameras.

The fields of view of the cameras can be evaluated via two primary methods. The first evaluation method employed the native capability of Autodesk 3ds Max to generate simulated camera views. For each camera, a rendering of what that camera would 'see' can be created and saved as an image file. Fig. 8 shows example simulated views for all four cameras. These camera views allowed us to evaluate whether any of the landing feet were visible to the cameras, which was one of the requirements of the SCALPSS design. The second evaluation method projected the camera views onto the ground, allowing the photogrammetric coverage of the ground to be determined. We did this by creating four rectangular point-source spotlights with angles of view identical to that of the cameras (93.1° by 76.8°) and overlapping these spotlights with the cameras. This served to project the views of each camera onto the scene, as shown in Fig. 7 (b). We used this method to evaluate the amount of area along the ground that was visible to photogrammetry: if a region on the ground was illuminated by lights from multiple cameras simultaneously, then multiple cameras could 'see' that region and thus photogrammetry could be performed there. Note that some of the lander geometry, such as the engine bell and landing legs, cast shadows in the spotlight projections. These shadows indicate regions on the ground that the cameras cannot see because they are obscured by the lander. This is a critical feature that aids in ensuring the representativeness of these coverage simulations. The ground plane was set to be a translucent material, so that the projected coverage of each virtual SCALPSS camera could be observed by another virtual camera placed below the ground plane, as shown in Fig. 9. An example view provided by this camera is shown in Fig. 10 (a). The following section describes how this additional camera view was used to gain more information about the performance of the camera system design.

The Autodesk 3ds Max environment also allowed sunlight and the resulting shadows to be simulated. Information about the landing date and site of the *Nova-C* on the Moon indicated that the Sun will appear to be approximately 10° above the eastern horizon, as viewed from the landing site. Based on this solar illumination geometry, virtual sunlight was created in the simulation environment. The resulting shadow cast by the lander is visible in Fig. 7 (a), and it can be seen that one of the landing legs casts a shadow directly across the photogrammetry region under the lander. One of the design constraints required that two of the cameras be located in the shade after landing, which is a condition that can be easily checked by inspecting the 3D scene.

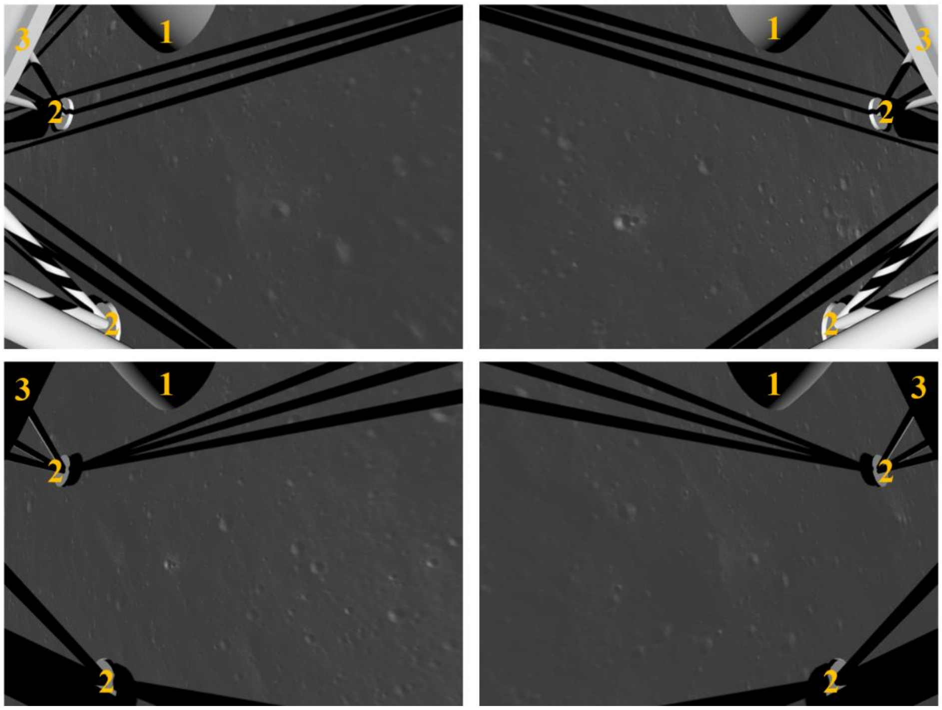

Fig. 8 Simulated post-landing SCALPSS camera views of the ground directly below the *Nova-C* lander. Shadows cast by the east-facing landing leg are visible across the top of each frame. The labeled components are: 1, the engine bell; 2, the landing feet; and 3, the lander body.

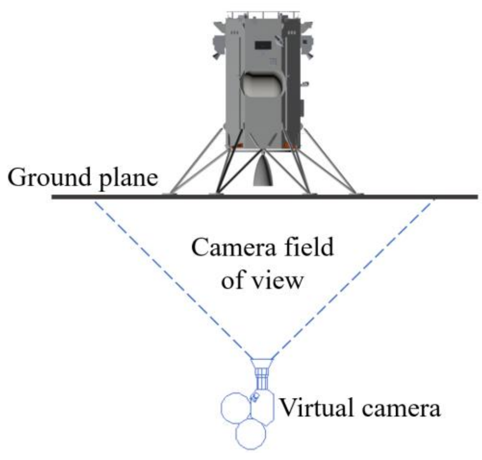

Fig. 9 Side view of the scene, showing the position of the bottom-view virtual camera that acquires images to map the stereo coverage provided by a camera configuration. The virtual camera was set to acquire undistorted images of the ground plane.

C. Processing Workflow

In order to perform photogrammetry using the SCALPSS camera system, two or more cameras must have overlapping views of the ground directly under the lander; this photogrammetric viewing region is hereafter referred to as stereo coverage or stereo area. For studying the plume-induced crater, a circular region 3.14 meters in diameter, centered under the descent engine, was somewhat arbitrarily deemed the "area of interest" (AOI) as the crater was expected to be contained in this region. Accurate measurements of the crater require as much of this AOI to be accessible to photogrammetry as possible. That is, the percent of area within the AOI (hereafter referred to as AOI percent coverage) that also falls within the stereo coverage region must be as high as possible. While two cameras viewing the same region of ground is the minimum for photogrammetric analysis, more than two cameras viewing the same region improves the accuracy of the measurement. High-performing camera configurations have large stereo coverage areas and a high AOI percent coverage, with as many cameras as possible viewing the region under the lander. If only total stereo coverage had been considered, coverage under the lander where the plume-induced crater forms would not have been guaranteed. Conversely, if only AOI percent coverage had been considered, visibility of the region outside the crater—which is necessary for assessing the flatness of the landing site—would not have been guaranteed. Thus, both metrics were considered in parallel to arrive at a camera system design that met the design constraints. We used these coverage metrics to assess the performance of a given camera configuration.

To evaluate a potential camera system design, we must first calculate the stereo coverage area and AOI percent coverage provided by that design. This process starts by acquiring an image of the translucent ground from below with the virtual camera shown in Fig. 9, while the fields of view of the virtual SCALPSS cameras are being projected as lights. The acquired image contains a 'map' of the region of ground visible to the SCALPSS cameras, an example of which is shown in Fig. 10 (a). In this example, the region near the edges of the image are black, indicating that they are not visible to any of the cameras. Regions of ground that are visible by one camera appear dark gray, and regions that are visible by more than one camera appear brighter shades of gray, depending on the number of cameras that can 'see' each region. This image, while informative on its own, can be made more useful through post-processing. In MATLAB, the image was imported, converted to grayscale, and several thresholds were applied to convert pixel values to the number of cameras that each pixel is visible to. The smallest pixel values were mapped to zero cameras, while the largest pixel values were mapped to four cameras, and so on. The physical size of each pixel on the ground was known, so we could calculate the total area that was accessible to photogrammetry by summing the number of pixels that were visible to two or more cameras. Additionally, by calculating how much of that area falls within the 3.14-meter-diameter AOI, we can determine the AOI percent coverage. The result of these processing steps is shown for an example camera configuration in Fig. 10 (b). In this example, a total area of 13.25 square meters, and 84% of the area in the AOI, is accessible to photogrammetry.

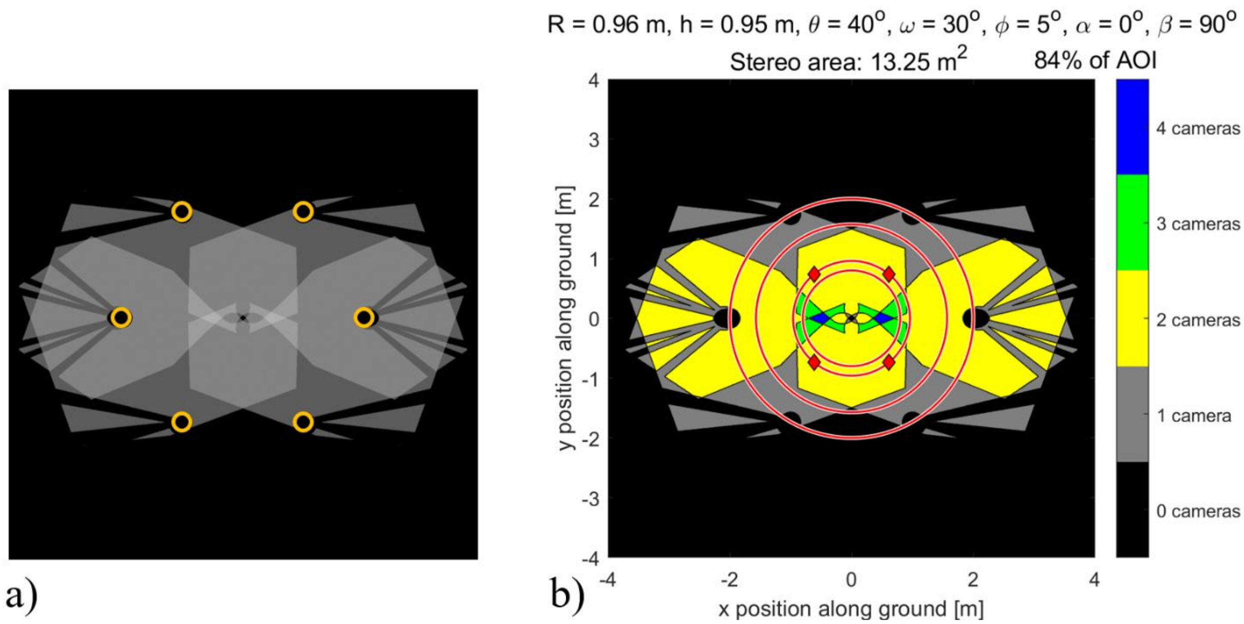

Fig. 10 a) Image acquired by the bottom-view virtual camera, showing the pattern of SCALPSS camera coverage of the ground under the lander. The superimposed yellow circles indicate the positions of the landing feet. b) Processed coverage map based on the image in (a). The camera coordinates for this configuration are shown at the top of the plot. The red diamonds mark the positions of the cameras. The red circles, from innermost to outermost, are the lander body circumscribed circle, the camera-mounting circle, the extents of the AOI, and the circumscribed circle of the footpads.

These steps were automated using MAXScript macros and MATLAB scripts so that many camera system designs could be tested quickly. A batch of camera configurations was passed to a MAXScript macro, and for each configuration, the macro placed the SCALPSS cameras accordingly and acquired an image using the bottom-view virtual camera. In MATLAB, each of these images—one for each camera configuration—was processed to produce a plot similar to Fig. 10 (b). The total computation time for each configuration was approximately 9 seconds, so around 400 configurations could be simulated and evaluated per hour. This processing speed lent itself to performing large searches of the available design space and optimization studies, which are discussed in further detail in Section V. B.

V. Simulation Results

The virtual environment described here allowed the photogrammetric performance of candidate SCALPSS camera configurations to be evaluated, accounting for obstructions to the camera views such as the *Nova-C* landing legs and descent engine nozzle. This proved to be an essential resource throughout the SCALPSS design stage, during which numerous configurations were developed, tested, and improved in the virtual environment. Frequent changes in the design of the *Nova-C* lander added another layer of complexity to the design of the camera system. However, these changes could be quickly incorporated in the analysis by importing updated models of the *Nova-C* lander into the environment. High-performing camera configurations were evaluated against the engineering constraints and further optimized using the environment. This process, after several iterations, resulted in the selection of a camera system design to be flown on the *Nova-C*.

A. Stereo Coverage Maps

After the release of the *Nova-C* version 1.0 geometry in January of 2020, a wide variety of SCALPSS camera system designs were simulated. The photogrammetric coverage of each of these designs was evaluated, which allowed the designs to be directly compared with each other. For many of these designs, coverage maps were generated. Two example coverage maps, which illustrate the variety of possible designs, are shown in Fig. 11. Designs that exhibited large total stereo coverage and AOI percent coverage were iteratively adjusted and optimized, as discussed in the next section. Two quantities—total stereo coverage and AOI percent coverage—were being optimized, but often a design that performed well based on one of the metrics did not perform well based on the other. For example, the camera configuration presented in Fig. 11 (b) exhibits a large AOI percent coverage, but a relatively small total stereo coverage. In response to this, we decided to pursue designs that performed relatively well with regards to both metrics. This process ultimately led to the discovery of a single camera configuration that provided a large stereo area and AOI percent coverage, and also satisfied all of the design constraints. This configuration was chosen as the final design and is discussed further in Section V. D.

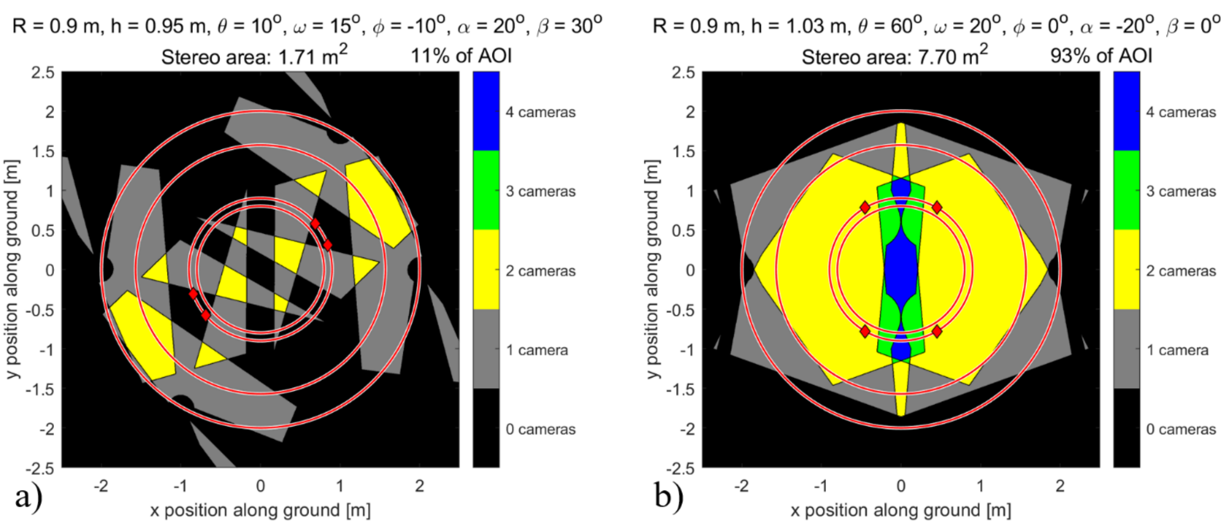

Fig. 11 a) An example of a poor-performing camera configuration. Both the total stereo coverage and the AOI percent coverage are significantly lower than most other configurations. b) A configuration that provides a large AOI percent coverage, but only an average total stereo area.

B. Optimization Studies

The simulation process presented here was automated to operate in a batch mode based on MAXScript macros and MATLAB scripts. As mentioned earlier, a single camera configuration could be simulated and evaluated in a few seconds, so large searches across the available design space were possible. Early in the design process, several of these searches were conducted in order to aid in the discovery of high-performing camera system designs. The largest search of this type evaluated nearly 23,000 different camera configurations and required about 56 hours of computation time. In this search, a test matrix was employed that varied every parameter within the bounds imposed by the design constraints. These searches revealed several different possible designs that provided both large AOI percent coverage and total stereo coverage. Each of these designs was investigated further and evaluated against the design constraints. One such design which satisfied all the necessary constraints was specified by $R = 1$ m, $h = 1.03$ m, $\theta = 40°$, $\omega = 30°$, $\phi = 5°$, $\alpha = 0°$, and $\beta = 30°$. To determine whether this configuration could be further improved, we conducted an optimization study. The parameters R, h, ω, ϕ, and α were kept constant, while θ was varied in the range [35°, 45°] and β was varied in the range [25°, 35°], both with 1° increments. For every combination of parameters within these ranges, the total stereo coverage and the AOI percent coverage were determined, and the results for total coverage area are plotted in Fig. 12. As can be seen in the figure, a local maximum exists at $\theta = 40°$ and $\beta = 30°$. Thus, these coordinates maximized the total stereo coverage provided by this configuration.

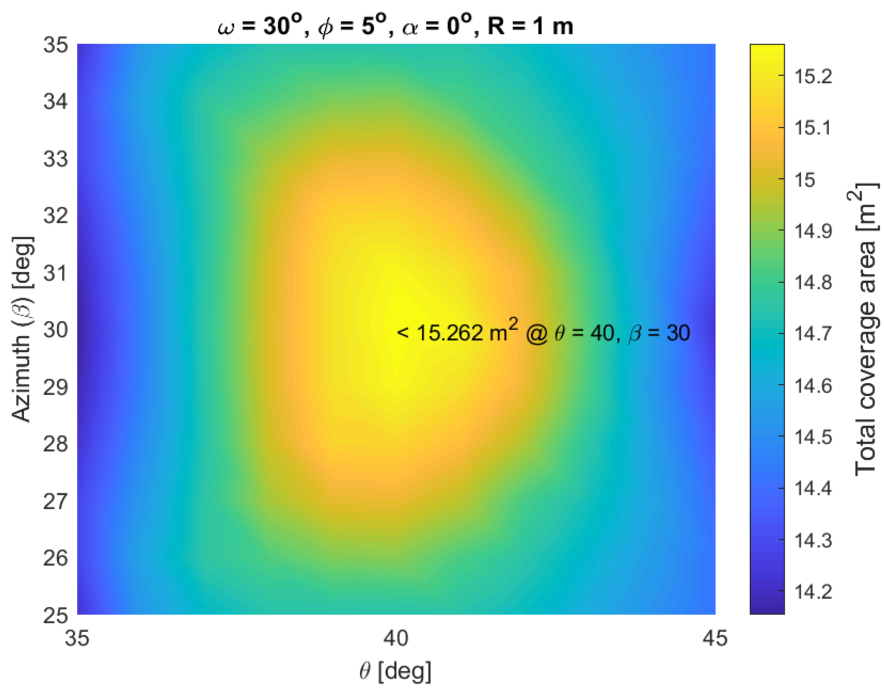

Fig. 12 Two-dimensional optimization of the total coverage area for a set of fixed parameters.

Later in the design process, in April of 2020, version 1.1 of the *Nova-C* lander geometry was released. In this update, the height of the lander body above the ground had been decreased slightly. As a result, the new lander body geometry obstructed a significant portion of the SCALPSS cameras' views. This necessitated the lowering of the SCALPSS cameras to compensate for the change in the height of the lander body. To determine the optimal distance that the cameras should be lowered, another optimization study was conducted. In this study, the camera height h was varied in the range [0.9 m, 1.03 m] while all the other parameters were kept constant. At each height, the total coverage area and the AOI percent coverage were simulated. Both metrics (total stereo area and AOI percentage) are plotted in Fig. 13. The optimization study revealed a local maximum of stereo coverage at $h = 0.95$ m and a local maximum of AOI percent coverage at $h = 0.98$ m. We decided that the camera mounting height should be reduced to $h = 0.95$ m, which provides a satisfactory combination of stereo coverage and AOI percent coverage. In addition, this mounting height would ensure that two landing feet would each be visible by two cameras, while the other four landing feet would each be visible by one camera. This is an example of the capability of the ViDI environment to enable fast adaptations to design changes and facilitate the quick development of simulations that inform design decisions.

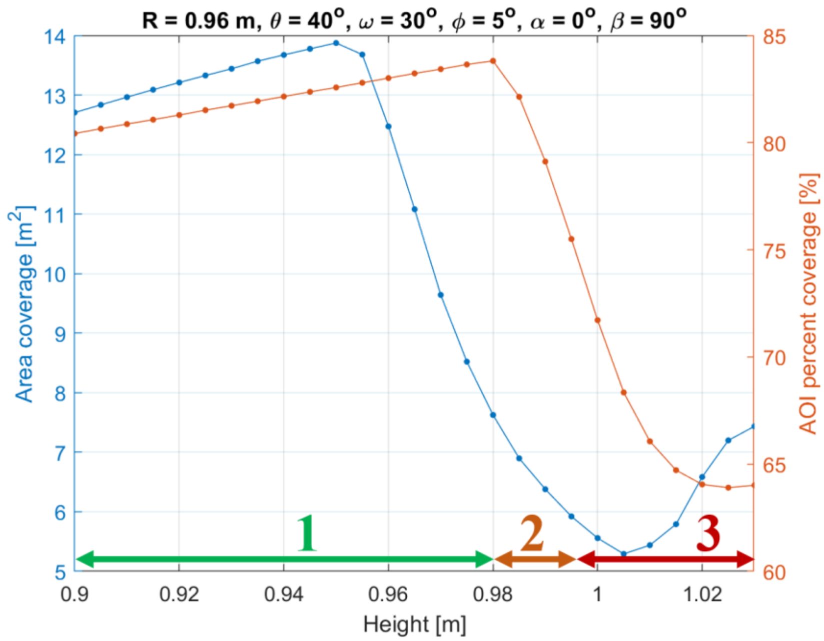

Fig. 13 One-dimension optimization of both stereo area coverage and AOI percent coverage. In region 1, two footpads are visible by two cameras and four footpads are visible by one camera. In region 2, two footpads are partially visible by two cameras and four footpads are visible by one camera. In region 3, four footpads are visible by one camera and no footpads are visible by two cameras.

C. Camera Views

Autodesk 3ds Max allows camera views to be simulated, which served as a source of qualitative information that aided in the design of the camera system. One of the design constraints is that as many of the landing feet as possible should be visible to the SCALPSS cameras. This would allow the cameras to monitor the landing legs for deflection during landing, which is a capability that is desirable to Intuitive Machines. Example rendered views for all four cameras are shown in Fig. 8. As can be seen in the simulated views, all six of the landing feet are visible to the SCALPSS cameras. In addition, the engine bell and small portions of the lander body are visible to the cameras. The visibility of the lander body was not initially a design constraint, but it is desirable because it would allow the orientation of each camera to be monitored during flight. If one of the cameras shifted during landing, for example, the shift could be monitored by examining how much the lander body appeared to shift in the camera's field of view. This was an unexpected design realization that occurred as a direct result of simulating the views of each of the SCALPSS cameras.

D. Final Configuration Decision

The camera configuration that was presented and optimized in Section V. B. was ultimately chosen as the final design for the SCALPSS science mission. The camera locations and orientations in this design are specified by the parameters in Table 2. The chosen design provides an estimated 13.25 square meters of stereo coverage, with 84% of the AOI accessible to photogrammetry. More than 30,00 total configurations were tested during the design process, and the chosen design performed in the top 1% of the tested configurations with respect to stereo coverage and the top 5% with respect to AOI percent coverage. The design also places two of the four cameras in the shadow of the *Nova-C* upon landing, which will protect them from intense sunlight to improve the longevity of these two cameras, and will enable photogrammetry under the lander even if two of the four become inoperative. In addition, the design employs a symmetric camera configuration, which simplifies the design and manufacturing of the camera mounting hardware. These mounts place the cameras approximately 25 centimeters from the body of the *Nova-C*, which is necessary for ensuring large stereo coverage. This placement satisfies the design constraint that the cameras must be mounted as closely as reasonably possible to the lander body to avoid damage from ejected rocks and dust during landing. These performance metrics are summarized for the chosen design inTable 3. The large stereo coverage and AOI percent coverage provided by this configuration, together with its satisfactory fulfillment of the design constraints, ultimately led to its selection as the final design.

The map of coverage provided by this configuration is shown in Fig. 10 (b). The simulated views of each camera in this configuration are shown in Fig. 8. The positions of two cameras and camera brackets are shown in Fig. 3 and Fig. 7 (a). The projected fields of view of the cameras in this design are shown in Fig. 7 (b).

Table 2 Parameters specifying the final design of the SCALPSS camera system.

Parameter	R [m]	H [m]	θ [°]	ω [°]	ϕ [°]	α [°]	β [°]
Value	0.96	0.95	40	30	5	0	90

Table 3 Critical design metrics and the performance of the final design with respect to each metric.

Metric	Total coverage area [m^2]	AOI coverage	Number of footpads within single-camera coverage	Number of footpads within stereo coverage	Lander body visible?	Two cameras in shadow?	Symmetric camera mounts?
Simulated result	13.25	84%	4	2	yes	yes	yes

VI. Conclusion

The SCALPSS camera system for studying the descent engine plume-surface interaction during the planned *Nova-C* lunar landing has been designed and analyzed in the 3D virtual environment described herein. The ViDI simulation environment allowed the testing of many thousands of possible designs and the optimization of the final chosen design. Using this system, the total stereo coverage area and AOI percent coverage were maximized subject to the required design constraints. SCALPSS simulations performed by MSFC and Cardinal Systems were independently validated and refined. In addition, ViDI facilitated fast implementation of design changes and provided a wealth of information that the design process significantly benefitted from. The final configuration of the SCALPSS cameras, placed in 3D space around the *Nova-C* lander model, was used to design precise mounting brackets for the cameras. This process has ensured that the camera system will meet all design constraints, integrate well with the *Nova-C* lander during assembly, and provide a large stereo coverage area under the lander. In addition to providing valuable engineering information, the ViDI environment provided visualizations that could be used for communication and public relations purposes. Future SCALPSS missions, after the October 2021 flight of the *Nova-C* lander, will likely be designed, in part, using this simulation environment. The operation of SCALPSS, if successful, will be the first dedicated plume-surface interaction measurement during an extraterrestrial landing.

Acknowledgments

The authors would like to acknowledge Intuitive Machines for providing 3D models of the *Nova-C* lander and contributing to valuable discussions regarding the design and operation of the SCALPSS camera system.

References

[1] Mehta, M., Sengupta, A., Renno, N.O., Van Norman, J.W., Huseman, P.G., Gulick, D.S., and Pokora, M., "Thruster Plume Surface Interactions: Applications for Spacecraft Landings on Planetary Bodies," *AIAA Journal*, Vol. 51, No. 12, 2013.

[2] Metzger, P.T., Immer, C.D., Donahue, C.M., Vu, B.T., Latta III, R.C., and Deyo-Svendsen, M., "Jet-Induced Cratering of a Granular Surface With Application to Lunar Spaceports," *J. Aerosp. Eng*., 22(1), pp. 24-32, 2009.

[3] Mehta, M., "Rocket Plume Interactions for NASA Landing Systems," [Presentation slides], 2019, URL: https://ntrs.nasa.gov/search.jsp?R=20200000979 [retrieved 22 May 2020].

[4] Smith, M., Craig, D., Herrmann, N., Mahoney, E., Krezel, J., McIntyre, N., Kandyce, G., "The Artemis Program: An Overview of NASA's Activities to Return Humans to the Moon," *IEEE Aerospace Conference*, 2020.

[5] Immer, C., Lane, J., Metzger, P., and Clements, S., "Apollo video photogrammetry estimation of plume impingement effects," *Icarus*, Vol. 214, No. 1, pp. 46-52, 2011.
doi: 10.1016/j.icarus.2011.04.018

[6] Schwartz, R.J. and Fleming, G.A., "Virtual Diagnostics Interface: Real Time Comparison of Experimental Data and CFD Predictions for a NASA Ares I-Like Vehicle," *2007 22nd International Congress on Instrumentation in Aerospace Simulation Facilities*, pp. 1-12, IEEE, 2007.

[7] Mehta, M., Manginelli, M., Liever, P.A., Gale, M., Westra, D., Thomas, O., "Simulation of InSight Plume Induced Surface Cratering and Validation Through Imagery Based 3D Topology Reconstruction," *16th International Planetary Probe Workshop* [Presentation slides], 2019.